DESIGN STUDY OF THE IMAGING BEAM LINE AT J-PARC MLF, *ERNIS*

Y. Kiyanagi[a*], T. Kamiyama[a], H. Sato[a], T. Shinohara[b], T. Kai[b], K. Aizawa[b], M. Arai[b], M. Harada[b], K. Sakai[b], K. Oikawa[b], M. Ohi[b], F. Maekawa[b], T. Sakai[b], M. Matsubayashi[b], M. Segawa[b], and M. Kureta[b]

[a] Faculty of Engineering, Hokkaido University, Kita-13, Nishi-8, Kita-ku, Sapporo, Hokkaido, 060-8628, Japan
[b] Japan Atomic Energy Agency, 2-4 Shirakata-shirane, Tokai-mura, Naka-gun, Ibaraki-ken, 319-1195, Japan

*Corresponding author: Prof. Yoshiaki Kiyanagi
kiyanagi@qe.eng.hokudai.ac.jp
Kita-13, Nishi-8, Kita-ku, Sapporo, Hokkaido, 060-8628, Japan.
Tel: +81-11-706-6650; Fax: +81-11-706-7368.

Abstract: We have a plan to build an imaging beam line, ERNIS (Energy-Resolved Neutron Imaging System), at MLF (Materials and Life Science Experimental Facility) at J-PARC (Japan Proton Accelerator Research Complex). In pulsed neutron imaging, we use characteristic features of the neutron total cross section, depending on the neutron wavelength, to get sample information such as crystallographic structure and nuclide composition. One of the most important items to be determined for a beam line at J-PARC is the choice of moderator among coupled, decoupled, and poisoned moderators. From the wavelength resolution point of view, we decided to use the decoupled moderator, which could cover major experiments performed at a pulsed neutron source. Here we discuss the structure of the imaging beam line at beam line 22 of the J-PARC neutron source as well as the arrangement of insertion devices and the experimental area.
Keywords: Pulsed neutron imaging, Imaging beam line at J-PARC, Bragg edge transmission, Resonance transmission, Magnetic transmission.

1. Introduction

The advent of energy-selective neutron imaging is expected to open a new field of neutron radiography. With steady state neutron sources, energy-

selective neutron imaging can result in different types of contrast imaging, depending on the total neutron cross section at the selective energy, which may provide more information regarding a sample than is given by other types of imaging. At the pulsed neutron source we can use the time-of-flight method (TOF) for the energy analysis. A two-dimensional position-sensitive detector combined with the TOF gives imaging data as a function of neutron flight time, namely, neutron wavelength. By analyzing this kind of transmission data we can obtain information on the crystal structure, texture, crystallite size, strain, nuclide composition, and magnetic field [1-4]. The pulsed neutron imaging is still under development. Once operational, it may produce more informative data than that of the traditional steady state neutron imaging due to its pulsed nature.

In Japan we have been developing the pulsed neutron imaging by using the small accelerator-based neutron source at Hokkaido University and the high-intensity pulsed neutron source, JSNS (Japan Spallation Neutron Source) at J-PARC MLF (Material Life Science Experimental Facility at the Japan Proton Accelerator Research Complex). The imaging beam line at J-PARC is expected to become one of the most intensive imaging beam lines in the world and to drastically promote the energy-resolved neutron imaging. We are now planning to build an imaging beam line at J-PARC.

Here, we present, as the first stage of design, the required resolution conditions for various kinds of imaging methods and the choice of the moderator type suitable for the imaging. We also discuss the structure of the beam line.

2. Required neutronic characteristics for an imaging beam line

For imaging at the pulsed neutron source we use TOF to analyze the neutron wavelength, and we need to know the required time resolution for each experiment. Here, we consider three types of measurement for the imaging so we can select the best moderator and the suitable flight path lengths for the beam line ERNIS at J-PARC MLF.

2.1 Bragg edge imaging

Bragg edge transmission (BET) spectra, shown in Fig. 1, obtained by a neutron imaging detector coupled with TOF spectroscopy at a pulsed source, can simultaneously and quantitatively give spatial distributions of crystal structure [1], crystalline phase [1], texture [2,3], microstructure [3], and strain [5] in a polycrystalline material. The preferred orientation information and the crystallite size information are included in the shape of a Bragg transmission spectrum corresponding to each Miller index, and the wavelength region to be used for analysis is from about 0.1 nm to larger than 1 nm, depending on the lattice spacing of the sample. A wavelength bandwidth of about 0.5 nm is used for analysis in many cases. The change of the shape around the Bragg edge is gentle. Therefore, the required wavelength resolution for the preferred orientation and the crystallite size is not so high, around 0.5%. This resolution is attainable by all moderators at the J-PARC neutron source. On the other hand, for the imaging of the lattice distance, the spatial dependent Bragg edge transmission spectra near the Bragg edge have to be analyzed precisely. Thus, the wavelength resolution required is very high, around 0.2%, as in the case of the high-resolution diffractometer, and users must have a code for analyzing the transmission data similar to the Pawley analysis method and the Rietveld analysis method used in TOF powder diffractometry. For the lattice spacing measurements, we had to carefully compare the performance obtained by each moderator.

Items to be considered are the (a) resolution of lattice spacing (d-spacing) $\Delta d/d$ for the strain refinements, (b) wavelength band width, (c) flux, and (d) beam collimation ratio, L/D. We aimed at obtaining a wavelength resolution of $\Delta d/d$ = 0.15% ~ 0.20% for strain imaging. This value came from the resolution of the strain/stress analysis diffractometer, TAKUMI [5], and the versatile powder diffractometer, iMATERIA [6], at J-PARC. In a Bragg edge transmission, $\Delta d/d$ equals $\Delta t/t$, where Δt is the FWHM (Full Width at Half Maximum) of a neutron pulse emitted from the moderator and t is the neutron flight time from the moderator to the detector. This holds for the transmission case, due to the fact that the Bragg edge corresponds to the Bragg angle of 90 degrees, namely a 180-degree scattering angle. Figure 2 shows the

calculation results for $\Delta d/d$ as a function of the flight distance at a neutron wavelength λ = 0.4 nm, which was estimated from the simulation data [6] for 4 type beam extractions from the 3 type moderators, that is, the coupled moderator (called CM, for the highest intensity), the decoupled moderator (DM, for medium resolution), and the poisoned moderator with an extraction from the thicker side (PM+, for higher resolution) and the thinner side (PM-, for the highest resolution). The beam line viewing PM- or PM+ can easily achieve the required resolution at the flight path length from 11.5 m to 20.5 m. In the case of a CM beam line, we need more than 68 m flight path length, and it is impossible to set such a long flight path in the present MLF building.

In Table 1, various performances of each beam line are summarized, assuming installation of a CM, DM, PM+, or PM- without supermirror guides. Here, we considered the $\Delta d/d$ = 0.20% case and the $\Delta d/d$ = 0.15% case estimated from the simulation data [7] and the experimental data [1,2,8] measured at the test port, NOBORU [9] viewing DM. We calculated the required flight path length by using pulse FWHM. Measurement times were calculated under the condition of the 1-mm pixel size, since in strain measurements the area measured is on the order of millimeters, while we will use detectors with higher spatial resolutions of several tens of micrometers. The wavelength bandwidths were determined by the 25-Hz repetition rate of the accelerator. The flight path length required for attaining the resolutions are over 68 m in the case of the CM, and with the other moderators the length ranges from 11.0 to 31.5 m. A length greater than 68 m is not realistic at J-PARC neutron source. For reference, the L/Ds in the case without a collimator are shown. The highest L/D is attained by this moderator, but the L/D is controllable by using the collimator. The attainable wavelength bandwidths are very narrow, about 0.2 nm. The Bragg cut-off (the longest-wavelength Bragg edge) usually appears at 0.4-0.7 nm, and we need the data at longer wavelengths above the Bragg-cut off and also the data of Bragg edges at shorter wavelengths. Therefore, the wavelength bandwidth required will be at least 0.5 nm, although it depends on the materials studied. Other characteristics of time-averaged intensities and measurement times are not so different each other. The CM is not suitable for the strain measurement. The

PM-, the PM+, and the DM based beam lines can give a relatively wide wavelength bandwidth owing to the shorter path length. At the same $\Delta d/d$ of 0.15% ~ 0.20%, the PM+ based beam line is the best choice because of its slightly higher intensity. However, the difference among the moderators is not very large, so all three moderator types other than the CM can be candidates for use.

Figure 1: Bragg edge transmission spectrum of a rolled α-Fe plate of 5 mm thickness, and crystallographic information obtained by its spectral analysis.

Figure 2: Wavelength resolution $\Delta d/d$ as a function of distance from the moderator to the detector at various beam lines viewing the four types of neutron emission surfaces.

Table 1: Summary of instrumental parameters of each beam line at 0.20% and 0.15% resolution.

2.2 Polarized neutron imaging

Visualization of the magnetic field is one of the most exciting applications for the neutron imaging technique, and the process is suited to use of a pulsed neutron source due to the TOF measurement. For example, this technique can be used to study the spatial magnetic field distribution inside a closed space or to visualize the magnetic domain structure of magnetic materials [4]. The neutron spin motion passing through a magnetic field is described by a simple equation, $\frac{\mathrm{d}}{\mathrm{d}t}\boldsymbol{\sigma}(t) = \gamma\boldsymbol{\sigma}(t) \times \boldsymbol{B}(t)$, where $\boldsymbol{\sigma}(t)$ is the unit vector parallel to the neutron spin, γ is the gyromagnetic ratio of the neutron, and $\boldsymbol{B}(t)$ is an external magnetic field. Accordingly, the neutron spin experiences a Larmor precession in a magnetic field with a frequency ω_L proportional to the magnetic field strength, and thus the precession angle φ can be written by the product of precession frequency ω_L and the flight time in the field. In other words, this angle φ depends on the path integral of the magnetic field in which neutrons traverse and on the neutron wavelength, λ. Thus, the monochromatized neutron beam is indispensable for the magnetic field imaging. In this sense, the usage of pulsed neutrons, which are intrinsically

monochromatic at each instant, gives us an opportunity to treat the strength of the magnetic field quantitatively, by studying the wavelength dependence of the transmitted neutron polarization using the TOF method with high efficiency. Moreover, we can obtain the information about the direction of the magnetic field by selecting the analyzing direction of neutron spins.

The requirements for the pulsed neutron beam line to perform the magnetic field imaging experiment using polarized neutrons are considered as follows. Here, we consider a magnetic field of the order of 10^{-4} to 10^{-1}T by using thermal to cold neutrons. First, in general, the usability of a broad wavelength bandwidth is necessary for the magnetic field imaging, because analyzing the neutron polarization in a broad wavelength range makes it possible to determine the magnetic field strength precisely. From the magnetic field sensitivity point of view, a longer wavelength neutron has an advantage when observing a weak magnetic field, as it stays for a long time in the field, while a shorter wavelength neutron is important when observing a stronger magnetic field. Here, we consider, as a realistic value, a wavelength band of about 1nm, and use a chopper system to obtain the succeeding wavelength region under the repetition rate of the J-PARC accelerator. Here, we consider the resolution depending on the wavelength, although we also should take into account other influences like the precision of the flippers, alignment of polarizer and analyzer or counting statistics which influence the angular resolution. Wavelength dependent change of the polarization is gentle as in the case of the shape around the Bragg edge. A wavelength resolution of around 0.5% is usable. However, it is desirable that the detection position can be changed depending on the field strength. For attaining this resolution, the DM is suitable for polarized neutron imaging.

2.3 Resonance imaging

The peak energies of the resonance neutron cross section are specific to a particular nuclide and the width is specific to the motion and temperature of the nuclide. Therefore, neutron resonance absorption spectroscopy (N-RAS) can provide information on the nuclides in a sample by analyzing the energies of the resonance transmission and on the dynamics of atoms (more precisely the nuclei of atoms) by analyzing the Doppler broadening of their resonance

cross section [10]. As such, the N-RAS can be applied to the microchemical analysis or dynamical analysis of the small amount of nuclide composition [11]. The TOF imaging at the resonance energy region gives the distribution of the neutron resonance absorption spectra at the corresponding sample position [12,13].

This kind of measurements using epi-thermal neutrons is suitable to a pulsed neutron source, since the intensity of the epi-thermal neutrons at the pulsed neutron source is much higher than that at the reactor source, and such measurements were already performed by using such detectors, Li glass detectors, GEM detectors, and MCP detector, which spatial resolutions range from few mm to 55 micro m. The measurement time is from few minutes to few hours depending on sample. and also on the spatial resolution. For carrying out such N-RAS imaging, we must consider factors such as the applied energy region and the energy resolution. The energy region needed for the N-RAS measurement is at least 1 to 1000 eV for chemical element analysis; for example, S has the minimum energy resonance peak at 200 eV and Cl at 400 eV. For the atomic dynamics characterization or the temperature measurement, we need the flight time resolution $\Delta t/t$ ~1% that can lead to the temperature resolution ΔT~10 K in the analysis using a Ta 4.28 eV peak. We have calculated instrumental parameters using moderator simulation results under such preconditions [7].

Figure 3 shows examples of calculated $\Delta t/t$ versus neutron flight path length for two neutron energies of around 4 and 400 eV. As shown in the figure, $\Delta t/t$ ~ 1% is achieved over 7 m of flight length at both energies for all moderator types. This dependency is the same up to 1000 eV. At less than 40 eV the DM moderator has the highest resolution, and at the higher energy region the resolution change among moderators disappears. The DM is better from the $\Delta t/t$ point of view.

The energy dependences of the pulse shapes are shown in Fig. 4. We did not include the effect of the time structure of the accelerator in these figures. In the low energy region, less than 100 eV, the DM has a fine shape with a higher peak. The CM has a broader peak width and a long tail, and the PM+ and PM- have slightly collapsed shapes. At higher energy their shapes

begin to resemble one another, but the CM has a broader half width than that of the others. The pulse shape is very important characteristics to analyze atomic dynamics and temperature. The DM is the best choice based on the neutron pulse shape.

For the chemical analysis, the peak separation ability in the high energy region is important. Especially, because at MLF, one neutron pulse is made from two proton bunches, which affects the resonance peak shape. We performed the resonance spectrum measurement on the beam line at MLF, and a peak split by the proton bunch was recognized. We estimate the peak split ability based on the spectrum. As one of measured data a 115-eV peak was confirmed to be split and this peak was used for evaluation of the resolution since this energy is close to the maximum energy we now can observe. The spectrum was obtained under the following conditions: flight length, 29 m; time channel width, 40 ns; proton bunch split, 599 ns. The rough estimate of the splitting energy from this result is twice that of the FWHM of the neutron pulse. When we use the DM, the energy resolution $\delta E/E$ becomes less than 1.8% at the flight length of 15 m, and less than 1% at 27 m.

We concluded that the DM beam line at the J-PARC MLF is the best choice for the N-RAS imaging. It is better one can choose a shorter flight path position for experiments requiring high intensity or a longer flight path for high-resolution experiments.

Fig. 3. Flight time resolution $\Delta t/t$ at neutron energy 3.9810 eV and 398.10 eV.

Fig. 4. Simulated peak shape at neutron energy 3.981 eV and 398.10 eV.

3. Beam Line Design

From the discussions in the previous section, only the strain measurement requires the poisoned moderator and other requirements match the performance of the decoupled moderator. The strain analysis is possible at a DM based beam line at a position of more than 20 m. Therefore, we decided to use the DM for the J-PARC imaging beam line. The wavelength resolutions are shown in Fig. 5 at the 15 m and 23 m positions. The resolutions are about 0.3% and 0.2% in the cold neutron region, respectively.

For this instrument to have the required characteristics, high flexibility is indispensable for the beam line design. Here, we explain the basic idea of the

beam line components and the experimental cave. Figure 6 is a preliminary but ideal drawing for the J-PARC beam line at present, assuming the use of beam line number 22; however, this structure may be changed after the final decision of the beam line number for the imaging.

We will now briefly discuss the elementary components of the proposed setup.

i) Shutter insert and bulk-shield insert

A Ni-coated natural neutron guide or low-Qc supermirror neutron guide with a cross section of 100 mm x 100 mm (= size of the moderator viewed surface) may be installed in a 2.3 to 7.3m section to increase the divergence of low-energy neutrons. This will be used only for high-intensity measurements.

ii) Rotary collimator

Beam divergence can be changed by use of a rotary collimator (RC) that will be installed at the uppermost stream of the experimental hall, which will make a pinhole at 7.7 m from the moderator, as shown in Fig. 6. The RC would have four holes; one is fully opened (i.e., 100 mm x 100 mm), and the others have different pinhole sizes. The pinhole will be made by steel and polyethylene. Its effectiveness has already been confirmed at NOBORU (BL10 of MLF).

iii) Bandwidth choppers and T0 chopper

A bandwidth chopper (BWC) will be installed to eliminate so-called frame overlap neutrons. Because the total flight path length changes considerably in this instrument, the bandwidth must be matched by phasing two counter-rotated BWCs.

The T0 chopper, which suppresses the high-energy neutrons and the gamma-ray flash coming mainly from the moderator, will be installed just after the BWCs. This chopper will be operated when thermal and/or cold neutron will be mainly used, whereas it will be stopped in the opening position for resonance neutron imaging experiments.

iv) Exchangeable optics

Exchangeable neutron optics parts will be installed following the choppers. The components such as filters (Bi, Cd, etc…), a polarizer with a spin flipper, a neutron lens system, Soller slits, and narrowers are now under consideration. These items will have to be switched as required.

v) Experimental area

If the pinhole will be made at the 7.7 m position in the rotary collimator, the beam size of 200 mm x 200 mm can be realized at L1 = 23.1 m. This position is just before the ‘Rearmost Position’ indicated in Fig. 6. Here, an L/D value of about 5000 can be achieved by use of a 3-mm pinhole at 7.7 m.

The ‘Forefront Position’ will be used for the high-intensity measurements such as real-time tomography. Low-energy neutrons down to 1 meV can be used easily at this position.

A sample stage consist of a goniometer should have sufficient load capacity, now we consider 1 ton. The stage is movable on the guide rail between forefront and rearmost positions. Adjustable vacuum pipe are required to minimize air scatter.

Floor space in the cave should be adequate, as shown in Fig. 6; however, 3.8 m may be the maximum height. Because a large volume sample could be highly radioactive, a temporary sample storage area should be allocated inside the experimental cave.

Fig. 5 Wavelength resolutions at the 15-m and 23-m positions.

Fig. 6 Preliminary beam line sketch including various insertion devices.

4. Conclusion

We have considered the design items for the imaging beam line at J-PARC MLF. Requirements of many applications matched the decoupled moderator performance. Therefore, we decided to use the beam line viewing the decoupled moderator and made a preliminary sketch of the imaging beam line. The letter of intent for the imaging beam line was submitted to J-PARC, and we have received permission to build an imaging beam line. Therefore, we will construct the beam line in the near future.

Acknowledgements

This work was partially supported by a Grant-in-Aid for Scientific Research (A) from the Japan Society for the Promotion of Science (No. 20246136).

References

[1] Y. Kiyanagi, H. Sato, O. Takada, N. Ayukawa, and T. Kamiyama, AccApp09 Proc. AP/AM-07.

[2] H. Sato, O. Takada, K. Iwase, T. Kamiyama, and Y. Kiyanagi, J. Phys.: Conf. Ser., 251 (1), (2010) 012070.

[3] K. Iwase, K. Sakuma, T. Kamiyama, and Y. Kiyanagi, Nucl. Instr. and Meth., **A605** (2009) 1.

[4] N. Kardjilov, I. Manke, M. Strobl, A. Hilger, W. Treimer, Th. Krist, and M. Meissner, Nature Physics 4, (2008) 399.

[5] S. Harjo, A. Moriai, S. Torii, H. Suzuki, K. Suzuya, Y. Morii, M. Arai, Y. Tomota, K. Akita, and Y. Akiniwa, Mater. Sci. Forum **524-525** (2006) 199.

[6] T. Ishigaki, A. Hoshikawa, M. Yonemura, T. Morishima, T. Kamiyama, R. Oishi, K. Aizawa, T. Sakuma, Y. Tomota, M. Arai, M. Hayashi, K. Ebata, Y. Takano, K. Komatsuzaki, H. Asano, Y. Takano and T. Kasao, Nucl. Instr. and Meth., **A600** (2009) 189.

[7] http://j-parc.jp/MatLife/en/instrumentation/ns3.html

[8] H. Sato, O. Takada, S. Satoh, T. Kamiyama, and Y. Kiyanagi, Nucl. Instr. and Meth. **A 623** (2010) 597.

[9] F. Maekawa, K. Oikawa, M. Harada, T. Kai, S. Meigo, Y. Kasugai, M. Ooi, K. Sakai, M. Teshigawara, S. Hasegawa, Y. Ikeda, and N. Watanabe, Nucl. Instr. and Meth., **A600** (2009) 335.

[10] K. Kaneko, T. Kamiyama, Y. Kiyanagi, T. Sakuma, and S. Ikeda, J. Phys. Chem. Solids, **60** (1999) 1499.

[11] T. Kamiyama, H. Noda, J. Ito, H. Iwasa, Y. Kiyanagi, and S. Ikeda, J. Neutron Research, 13 (2005) 97.

[12] T. Kamiyama, J. Ito, H. Noda, H. Iwasa, Y. Kiyanagi, and S. Ikeda, Nucl. Instrum. and Methods, **A 542** (2005) 258.

[13] H. Sato, T.Kamiyama, and Y. Kiyanagi, Nucl. Instr. and Meth, **A 605** (2009) 36.

FIGURE CAPTION LIST

Fig. 1: Bragg edge transmission spectrum of a rolled α-Fe plate of 5 mm thickness, and crystallographic information obtained by its spectral analysis.

Fig. 2: Wavelength resolution $\Delta d/d$ as a function of distance from the moderator to the detector at various beam lines viewing the four types of neutron emission surface.

Fig. 3: Flight time resolution $\Delta t/t$ at neutron energy 3.9810 eV and 398.10 eV.

Fig. 4: Simulated peak shape at neutron energy 3.981 eV and 398.10 eV.

Fig. 5: Wavelength resolutions at the 15-m and 23-m positions.

Fig. 6: Preliminary beam line sketch of the imaging instrument.

TABLE CAPTION LIST

Table 1: Summary of instrumental parameters of each beam line at 0.20% and 0.15% resolution.

Figure 1

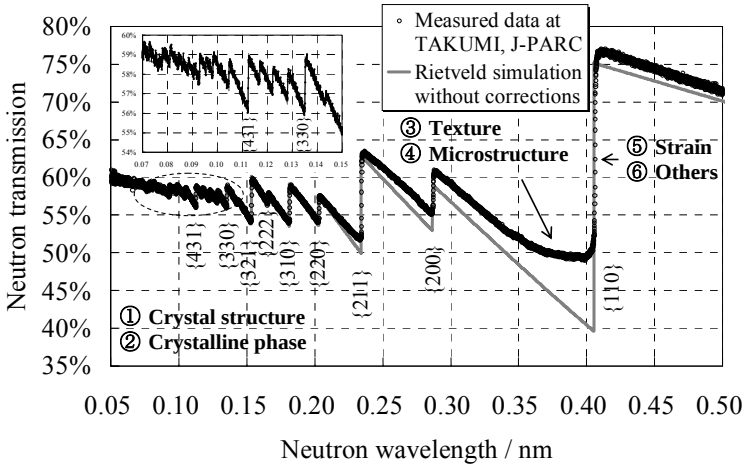
Measured data at TAKUMI, J-PARC
Rietveld simulation without corrections
③ Texture
④ Microstructure
⑤ Strain
⑥ Others
① Crystal structure
② Crystalline phase
{431}
{330}
{321}
{222}
{310}
{220}
{211}
{200}
{110}
Neutron transmission
Neutron wavelength / nm
80%
75%
70%
65%
60%
55%
50%
45%
40%
35%
0.05
0.10
0.15
0.20
0.25
0.30
0.35
0.40
0.45
0.50

Figure 2

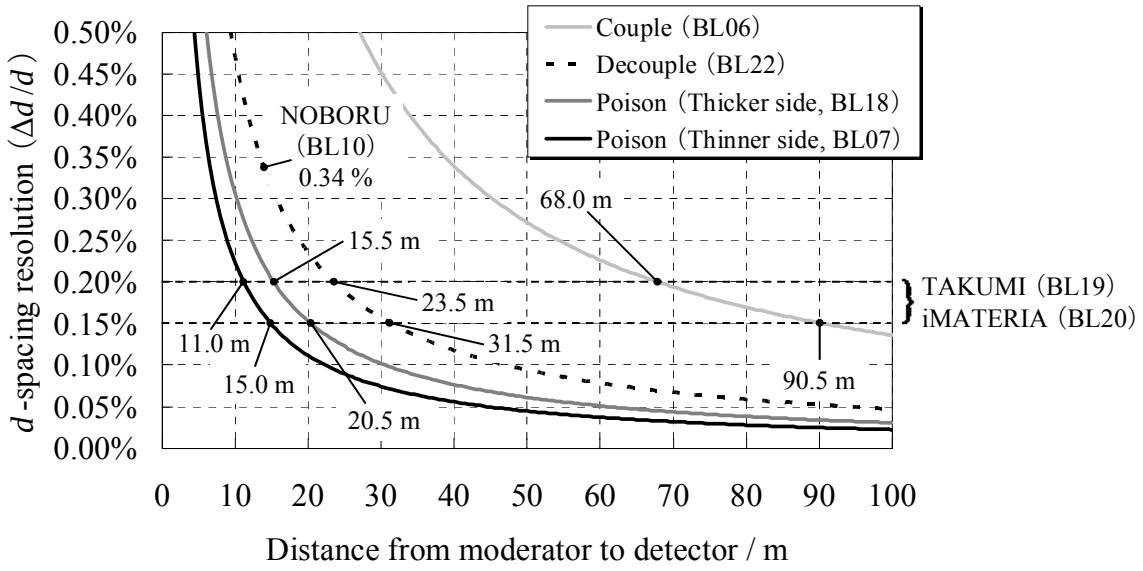
Couple（BL06）
Decouple（BL22）
Poison（Thicker side, BL18）
Poison（Thinner side, BL07）
NOBORU
（BL10）
0.34 %
68.0 m
15.5 m
23.5 m
31.5 m
90.5 m
11.0 m
15.0 m
20.5 m
TAKUMI（BL19）
iMATERIA（BL20）
d -spacing resolution（Δd /d）
0.50%
0.45%
0.40%
0.35%
0.30%
0.25%
0.20%
0.15%
0.10%
0.05%
0.00%
0
10
20
30
40
50
60
70
80
90
100
Distance from moderator to detector / m

Figure 3

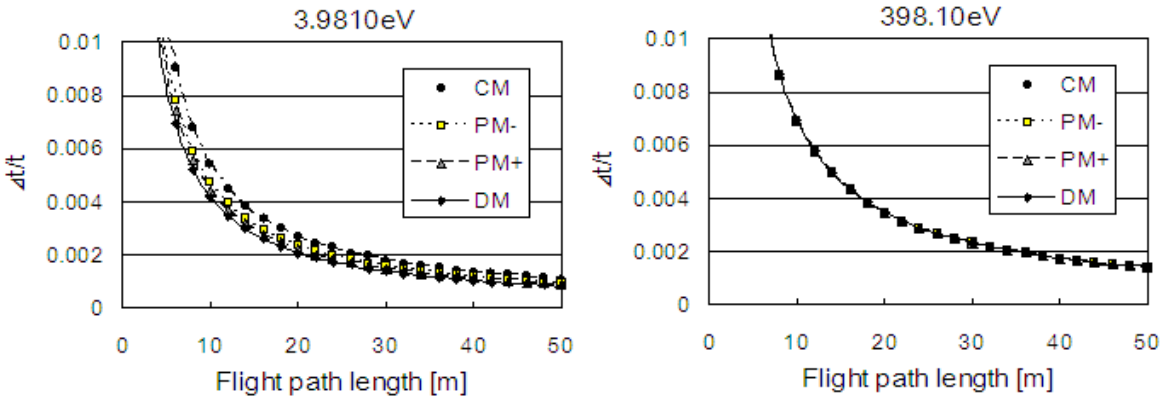
3.9810eV
0.01
0.008
0.006
0.004
0.002
0
Δt/t
0
10
20
30
40
50
Flight path length [m]
CM
PM-
PM+
DM
398.10eV
0.01
0.008
0.006
0.004
0.002
0
Δt/t
0
10
20
30
40
50
Flight path length [m]
CM
PM-
PM+
DM

Figure 4

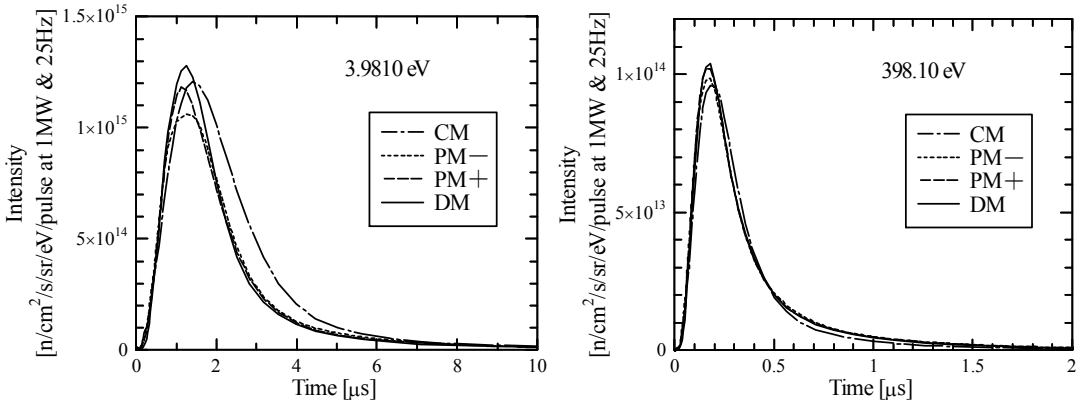
3.9810 eV
CM
PM−
PM+
DM
Intensity
[n/cm2/s/sr/eV/pulse at 1MW & 25Hz]
Time [μs]
398.10 eV
CM
PM−
PM+
DM
Intensity
[n/cm2/s/sr/eV/pulse at 1MW & 25Hz]
Time [μs]

Figure 5

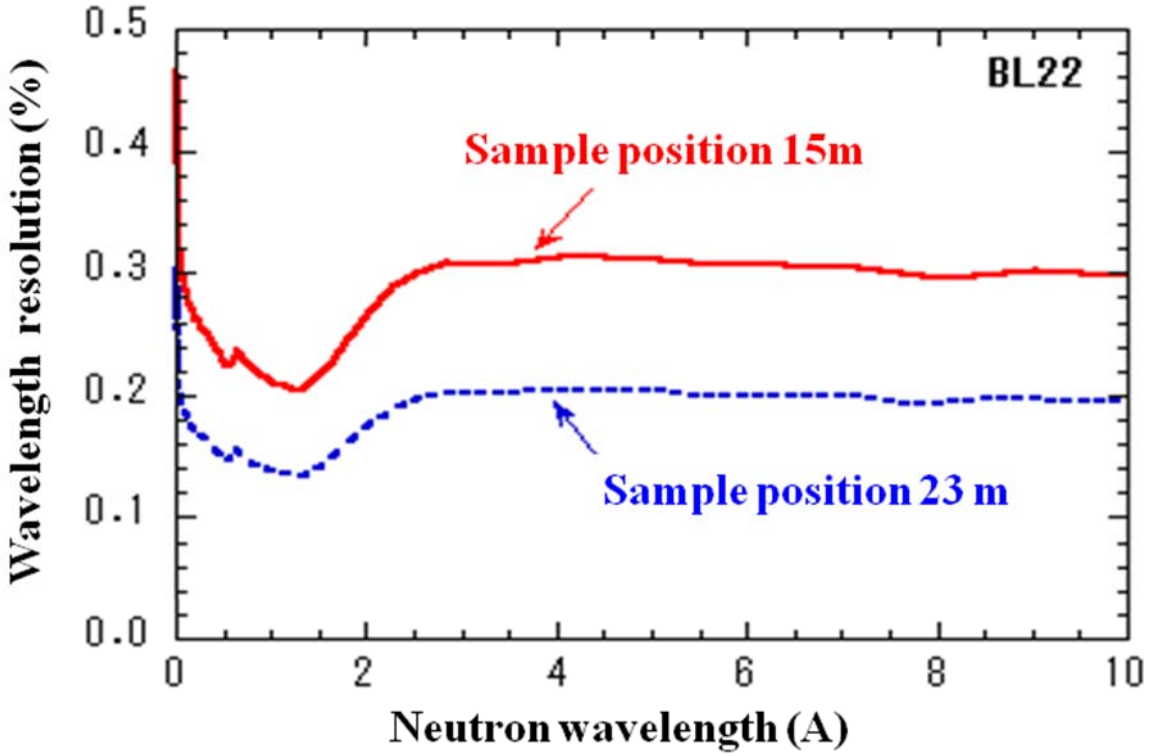
BL22
Sample position 15m
Sample position 23 m
Wavelength resolution (%)
Neutron wavelength (A)
0.0
0.1
0.2
0.3
0.4
0.5
0
2
4
6
8
10

Figure 6 Preliminary beam line sketch of the imaging instrument.

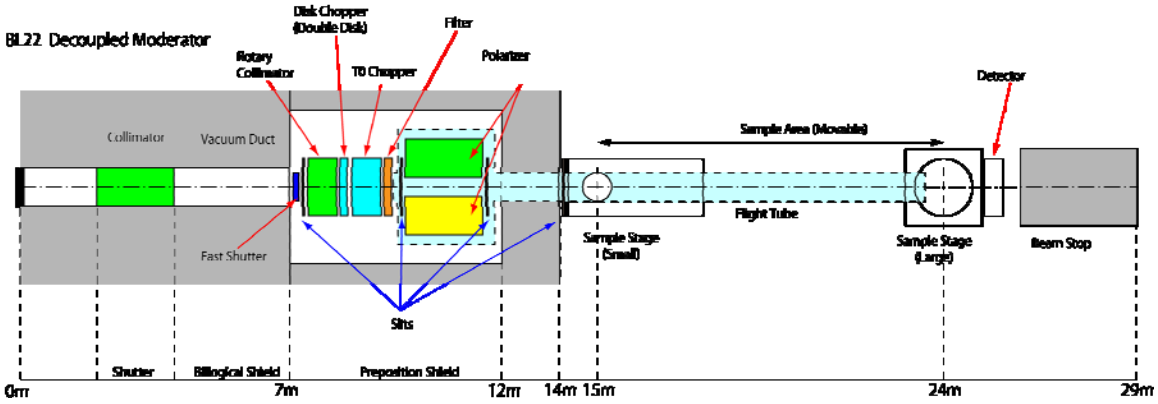

Table 1

Choice of moderator and flight path length for achieving $\Delta d/d$ of 0.20 % or 0.15 %	**CM（BL06）** 68.0 m / 90.5 m	**DM（BL22）** 23.5 m / 31.5 m	**PM+（BL18）** 15.5 m / 20.5 m	**PM-（BL07）** 11.0 m / 15.0 m
Available wavelength band limit @ 25 Hz / nm	0.23 / 0.17	0.67 / 0.50	1.02 / 0.77	1.44 / 1.05
Time-averaged cold neutron flux / $cm^{-2}s^{-1}$	1.3×10^{7} / 7.5×10^{6}	1.6×10^{7} / 7.7×10^{6}	1.8×10^{7} / 9.9×10^{6}	1.7×10^{7} / 8.8×10^{6}
Pulse FWHM Δt @ 0.4 nm / μs	138.5	48.0	31.2	22.7
Beam collimation ratio *L*/*D* without pinholes	680 / 905	235 / 315	155 / 205	110 / 150
Measurement time of strain imaging / min for 1 mm^2/pixel & $\Delta t\times0.05$ μs TOF-analysis in case of 10000 counts for 0.4 nm neutrons	27.0/ 63.7	25.7 / 61.9	24.4 / 56.3	26.3 / 66.5
Measurement time of the others imaging / min for 1 mm^2/pixel & $\Delta t\times0.5$ μs TOF-analysis in case of 5000 counts for 0.4 nm neutrons	1.4 / 3.2	1.3 / 3.1	1.2 / 2.8	1.3 / 3.3